ARTICLE

E3 ligase *FBXW7* aggravates TMPD-induced systemic lupus erythematosus by promoting cell apoptosis

Zhenlu Chong[1], Chunjing Bao[1], Jia He[1], Tianxiao Chen[1], Lijia Zhong[2], Gaopeng Li[1], Huanle Li[1], Lutong Fang[1], Yinjing Song[1], Guoxiang Fu[3], Xuyan Yang[4], Lihua Lai[1], Yang Liu[1] and Qingqing Wang[1]

Systemic lupus erythematosus (SLE) is a systemic autoimmune disease, and the pathogenesis of SLE has not been fully elucidated. The E3 ubiquitin ligase *FBXW7* has been well characterized in cancer as a tumor suppressor that can promote the ubiquitination and subsequent degradation of various oncoproteins; however, the potential role of *FBXW7* in autoimmune diseases is unclear. In the present study, we identified that *FBXW7* is a crucial exacerbating factor for SLE development and progression in a mouse model induced by 2, 6, 10, 14-tetramethylpentadecane (TMPD). Myeloid cell-specific *FBXW7*-deficient ($Lysm^{+}FBXW7^{f/f}$) C57BL/6 mice showed decreased immune complex accumulation, glomerulonephritis, glomerular mesangial cell proliferation, and base-membrane thickness in the kidney. $Lysm^{+}FBXW7^{f/f}$ mice produced fewer anti-Sm/RNP and anti-ANA autoantibodies and showed a decreased MHC II expression in B cells. In $Lysm^{+}FBXW7^{f/f}$ mice, we observed that cell apoptosis was reduced and that fewer $CD11b^{+}Ly6C^{hi}$ inflammatory monocytes were recruited to the peritoneal cavity. Consistently, diffuse pulmonary hemorrhage (DPH) was also decreased in $Lysm^{+}FBXW7^{f/f}$ mice. Mechanistically, we clarified that *FBXW7* promoted TMPD-induced cell apoptosis by catalyzing MCL1 degradation through K48-linked ubiquitination. Our work revealed that *FBXW7* expression in myeloid cells played a crucial role in TMPD-induced SLE progression in mice, which may provide novel ideas and theoretical support for understanding the pathogenesis of SLE.

Keywords: Systemic lupus erythematosus; apoptosis; *FBXW7*; MCL1; ubiquitination

Cellular & Molecular Immunology (2018) 15:1057–1070; https://doi.org/10.1038/s41423-018-0167-z

INTRODUCTION

Systemic lupus erythematosus (SLE) is a chronic autoimmune disease characterized by the loss of self-tolerance and production of autoantibodies against self-antigens, such as double-stranded (ds) DNA and components of small nuclear ribonucleoproteins, leading to immune complex deposition and multiple organ damage with the main complication of lupus nephritis.[1,2] The pathogenesis of SLE is not clearly understood. Multiple factors have been shown to contribute to SLE, including environmental, genetic susceptibility, hormone, and stochastic factors.[3,4] Many observations have provided new insight into the mechanisms involved in immune dysregulation and the loss of self-tolerance, such as deficiency in apoptotic cell clearance, nucleic acid sensing, lymphocyte activation, and type I interferon (IFN-I) production.[5] Notably, increased apoptosis and the defective clearance of dying cells triggering the activation of the innate immune system and driving the autoimmune response have attracted increasing attention in SLE pathogenesis.[5–7] This condition leads to the release of nuclear acids from cells that could be sensed by pattern recognition receptors (PRRs) to stimulate IFN-I production.[8] Recent evidence showed that patients with SLE present elevated IFN-I levels.[9–11] This "IFN signature" is supposedly associated with SLE pathogenesis, but IFN-I etiology in SLE is not fully understood. Various mouse SLE models have been applied to investigate this disease, including spontaneous models, such as NZB × NZW F1, MRL-lpr/lpr mice, and drug-induced models.[12–16] 2, 6, 10, 14-tetramethylpentadecane (TMPD), which is also known as pristine, has been widely used to induce murine models of SLE.[17–20] TMPD-treated mice show many clinical features of human lupus, including glomerulonephritis, arthritis, immune complex deposition, and autoantibody production.[19] TMPD-induced apoptosis is considered a critical initial event in the pathogenesis of SLE, which depends on IFN-I signaling.[19,21]

Ubiquitination is a widely existing post-translational protein modification that is involved in numerous cellular processes, including cell cycle progression, cell apoptosis, and innate immunity.[22–25] Ubiquitin consists of 76 amino acids and is a highly conserved polypeptide in eukaryotes.[26] Protein ubiquitination depends on the sequential action of the following three different classes of enzymes: ubiquitin-activating enzymes (E1s); ubiquitin-conjugating enzymes (E2s); and ubiquitin-ligating enzymes (E3s).[27] The E1s activate ubiquitin for conjugation, which depends on ATP, and transfer ubiquitin to E2. The E2 enzymes interact with E3 and attach ubiquitin to the targeted protein.[23]

[1]Institute of Immunology, Zhejiang University School of Medicine, 866 Yuhangtang Road, Hangzhou 310058, China; [2]The Children's Hospital, Zhejiang University School of Medicine, Hangzhou 310006, China; [3]Sir Run Shaw Hospital, Zhejiang University School of Medicine, Hangzhou 310016, China and [4]Department of Rheumatology, Second Affiliated Hospital, Zhejiang University School of Medicine, Hangzhou 310009, China
Correspondence: Yang Liu (liuyang0620@zju.edu.cn) or Qingqing Wang (wqq@zju.edu.cn)
These authors contributed equally: Zhenlu Chong, Chunjing Bao

Received: 26 April 2018 Accepted: 17 August 2018
Published online: 1 October 2018

The targeted proteins can be modified on one or more sites of the seven lysine residues with monoubiquitination or polyubiquitination, and lysine 48 (K48)- and lysine 63 (K63)-linked polyubiquitination is the most well characterized. Substrates with a former ubiquitin configuration are mainly degraded by the ubiquitin-proteasome system (UPS), while K63-linked modification is usually implicated in DNA repair, the inflammatory response, and protein translation.[28,29] Ubiquitin can also conjugate at lysine 6, lysine 11, lysine 27, lysine 29, lysine 33, and methionine (Met 1); however, the biological functions of these topologies of linkages are unclear.[27] In addition, ubiquitination is a reversible modification, and the polyubiquitin chains can be disassembled by deubiquitylation enzymes from targeted proteins.[30] Notably, the E3 ubiquitin ligase F-box and WD repeat domain-containing 7 (*FBXW7*), which is known as a tumor suppressor, target numerous well-known oncoproteins, including c-Myc, cyclin E, and Notch, for K48-linked polyubiquitination-mediated degradation.[31–35] The substrates of *FBXW7* generally contain a conserved Cdc4 phosphodegron (CPD) sequence and have to be properly phosphorylated by some kinases for *FBXW7* recognition.[23] A recent report discovered that *FBXW7* could attenuate Toll-like receptor (TLR)-mediated innate immune responses by down-regulating CCAAT/enhancer-binding protein delta.[36] Our previous study found that during RNA virus infection, *FBXW7* could catalyze SHP2, which is a negative regulator of IFN-I production, for K48-linked polyubiquitination and subsequent degradation. Consequently, *FBXW7* promoted IFN-I production by stabilizing RIG-I.[37] These discoveries highlight the role of *FBXW7* in regulating innate immunity and related diseases. However, the role of *FBXW7* in the pathogenesis of SLE has not been described.

Here we report that myeloid cell-specific *FBXW7*-deficient (Lysm^{+}*FBXW7*$^{f/f}$) C57BL/6 mice exhibit decreased immune complex deposition in the kidney and ameliorative lupus nephritis. Anti-Sm/RNP and anti-ANA autoantibodies were also significantly decreased in Lysm^{+}*FBXW7*$^{f/f}$ mice. During the acute stage, Lysm^{+}*FBXW7*$^{f/f}$ mice showed reduced cell apoptosis in the peritoneal cavity and decreased infiltration of CD11b^{+}Ly6C^{hi} inflammatory monocytes. *FBXW7* could promote TMPD-induced cell apoptosis, and this regulation was mediated by MCL1. MCL1 could be targeted by *FBXW7* for degradation through UPS. Collectively, our findings highlight the role of *FBXW7* in the regulation of SLE progression and provide new insight into the mechanism of SLE.

MATERIALS AND METHODS

Mice and TMPD induction of SLE model

FBXW7$^{f/f}$ mice on a C57BL/6J background were obtained from Jackson Laboratories. The Lysm-Cre C57BL/6J mice were kindly provided by Dr. Ximei Wu, Zhejiang University School of Medicine. All mice were housed at the University Laboratory Animal Center in a specific-pathogen-free environment and used at 8–10 weeks of age. All animal experiments were performed according to the protocol approved by the Animal Ethics Committee of Zhejiang University in compliance with institutional guidelines.

For the SLE induction, *FBXW7*$^{f/f}$ and Lysm^{+}*FBXW7*$^{f/f}$ mice received one intraperitoneal (i.p.) injection of 0.5 mL TMPD or phosphate-buffered saline (PBS; as a control), and survival was monitored for 6 months. For the ex vivo analysis, the experimental mice were sacrificed at the indicated time.

Cell lines and primary macrophages

The Raw264.7, 293T, and HeLa cells were obtained from American Type Culture Collection (ATCC) and maintained in Dulbecco's modified Eagle medium (DMEM) with 10% fetal bovine serum (FBS; Gibco). The THP-1 cells were obtained from ATCC and maintained in RPMI-1640 medium with 10% FBS. The thioglycolate (Merk)-elicited mouse peritoneal macrophages were cultured in RPMI-1640 medium with 10% FBS. Bone marrow-derived macrophages (BMDMs) were generated with recombinant mouse macrophage colony-stimulating factor (20 ng/mL) in RPMI-1640 medium with 10% FBS.

Antibodies and reagents

Antibodies against HA-tag (sc-805), Myc-tag (sc-40), Flag-tag (sc-807), β-actin (sc-130619), and ubiquitin (sc-271289) were obtained from Santa Cruz. Antibodies specific for Bcl2, Bax, cleaved caspase-3, and cyclin E were obtained from Cell Signaling Technology. The anti-MCL1, anti-*FBXW7*, anti-IgG, and anti-C3 antibodies were obtained from Abcam. The anti-CD11b-APC antibody, anti-CD11b-PE antibody, anti-Ly6C-FITC antibody, anti-Ly6C-PerCP Cy5.5 antibody, anti-Ly6G-PE antibody, anti-Ly6G-PB antibody, anti-CD11C-APC antibody, anti-B220-FITC antibody, anti-CD4-APC antibody, anti-CD8-PE antibody, anti-CD69-FITC antibody, and anti-MHC II-PE antibody were obtained from BioLegend. The anti-F4/80-FITC antibody, anti-CD45.1-FITC antibody, and anti-CD45.2-APC antibody were obtained from eBioscience.

MG132 (M8699), chlorhexidine (C4859), TMPD (P2870), and Flag M2 Magnetic Beads (M8823) were obtained from Sigma-Aldrich. The enzyme-linked immunosorbent assay (ELISA) kits for mouse IFN-α (luex-mifnα) were obtained from InvivoGen. The ELISA kits for mouse interleukin-6 (IL-6; BMS603HS), tumor necrosis factor-α (TNF-α; BMS607-3), and CCL2 (BMS6005) were obtained from eBioscience.

Quantitative reverse transcription–PCR

The total RNA was isolated from the cells using TRIzol reagent (Takara) according to the manufacturer's directions, and single-strand cDNA was generated from the total RNA and reverse transcriptase (Toyobo). The SYBR Green master Rox (Roche) was used for the quantitative real-time reverse transcription–PCR analysis according to the manufacturer's protocol. The sequences used for the primers are shown in Table 1.

ELISA assay

IFN-α, IL-6, TNF-α, and CCL2 were detected with ELISA kits (eBioscience) according to the manufacturer's protocols.

Flow cytometry

Single-cell suspensions containing 1×10^5 to 1×10^6 cells obtained from the peritoneal cavity, bronchoalveolar lavage fluid (BALF), spleen, and kidney were blocked with anti-CD16/CD32 antibodies and then stained with the indicated antibodies for 20 min at 4 °C. Then, the cells were washed with PBS once and resuspended

Table 1. Primers used for RT-PCR

m β-actin	F (forward):	AGTGTGACGTTGACATCCGT
	R (reverse):	GCAGCTCAGTAACAGTCCGC
m IFN-α	F:	TACTCAGCAGACCTTGAACCT
	R:	CAGTCTTGGCAGCAAGTTGAC
m IRF7	F:	GAGACTGGCTATTGGGGGAG
	R:	GACCGAAATGCTTCCAGGG
m ISG15	F:	GGTGTCCGTGACTAACTCCAT
	R:	TGGAAAGGGTAAGACCGTCCT
m MX1	F:	GACCATAGGGGTCTTGACCAA
	R:	AGACTTGCTCTTTCTGAAAAGCC
m IFN-γ	F:	ATGAACGCTACACACTGCATC
	R:	CCATCCTTTTGCCAGTTCCTC
m CCL2	F:	TTAAAAACCTGGATCGGAACCAA
	R:	GCATTAGCTTCAGATTTACGGGT

with PBS for flow cytometry. The flow cytometric analysis was conducted with FlowJo software (Tree Star).

Isolation of kidney cells

Freshly isolated kidneys were placed in ice-cold DMEM mixed with Hams F12 (1:1 ratio; Life Technologies, Grand Island, NY) on a 60-mm dish. The kidney capsule was removed by peeling with forceps, and the kidney was sliced coronally and homogenized by mincing into 1–2 mm^3 pieces. The homogenized kidney tissue pieces were resuspended and mixed in 10 ml of collagenase type I for 30 min to obtain single-cell suspensions. After digestion, the cell suspension was filtered through 70-μm cell strainers. The filtered cell suspensions were centrifuged at 300 × *g* for 2 min at 4 °C. The pellet was incubated with ACK lysing buffer (Beyotime Biotechnology) for 2 min at room temperature to remove red blood cells (RBCs) and centrifuged at 1000 × *g* for 5 min at 4 °C. Then, the pellet was washed with PBS containing 1% bovine serum albumin (BSA) and 0.1% sodium azide (Sigma-Aldrich) and passed through a 40-μm cell strainer. Then, the cells were prepared for staining and the flow cytometry analysis.

Plasmid constructs and transfection

Recombinant vectors encoding mouse *FBXW7* (NM_001177773) and MCL1 (NM_008562.3) were created by PCR-based amplification of RAW264.7 cDNA, followed by subcloning into the pcDNA3.1 eukaryotic expression vector (Invitrogen). The constructs were confirmed by DNA sequencing. The plasmids were transfected into 293T cells or HeLa cells with JetPrime (Polyplus) according to a standard protocol.

Co-immunoprecipitation assay and immunoblot analysis

For the co-immunoprecipitation assay, the cell extracts were prepared by using IP Lysis Buffer (Pierce, 87785) supplemented with protease inhibitor "cocktail" (Sigma, P8340). The cell lysates were centrifuged for 15 min at 12 000 × *g*, and the supernatants were incubated with Flag M2 Magnetic Beads overnight at 4 °C. The immunoprecipitates were washed three times with the same lysis buffer and eluted with 2× SDS loading buffer by boiling for 5 min. Then, the eluted immunoprecipitates were subjected to an immunoblot analysis.

For the immunoblot analysis, the cells were lysed with cell lysis buffer (Cell Signaling Technology, 9803) supplemented with a protease inhibitor "cocktail" (Sigma, P8340). The protein concentrations in the extracts were measured by a BCA assay (Pierce, 23235). Equal amounts of extracts per sample were subjected to SDS-polyacrylamide gel electrophoresis. Then, the resolved proteins were electrically transferred to a polyvinylidene fluoride membrane (Bio-Red). The immunoblots were probed with the indicated antibodies. The protein bands were visualized by using a Pierce chemiluminescence ECL kit (Thermo).

Statistical analysis

The statistical analysis was carried out with Prism 5. All data are shown as the mean ± S.E.M. The mean values of the biochemical data of each group were compared by Student's *t*-test. In the mouse survival study, Kaplan-Meier survival curves were generated and analyzed for statistical significance. p-Values < 0.05 were considered statistically significant.

RESULTS

FBXW7 deficiency attenuated immune complex deposition and nephritis in TMPD-induced SLE model

To investigate the role of *FBXW7* in the regulation of murine lupus, we generated myeloid cell-specific *FBXW7*-deficient ($Lysm^+FBXW7^{f/f}$) C57BL/6 mice. By analyzing the cell subsets in the bone marrow and lymph organs of 8- to 10-week-old mice, we found that the percentages of myeloid cells and lymphocytes were comparable between $FBXW7^{f/f}$ and $Lysm^+FBXW7^{f/f}$ mice (Supplementary Fig. 1). Thus, *FBXW7* deficiency in myeloid lineage does not affect the differentiation and development of myeloid cells and lymphocytes. Then, we injected TMPD into $FBXW7^{f/f}$ and $Lysm^+FBXW7^{f/f}$ mice to establish a murine SLE model. After the 6-month TMPD treatment, the mice were sacrificed, and the complement and autoantibody deposition in the kidney were detected. The results indicated that C3 and IgG deposition was significantly decreased in $Lysm^+FBXW7^{f/f}$ mice compared with that in $FBXW7^{f/f}$ mice (Fig. 1a). The electron micrograph also showed less immune complex deposition in the glomeruli endothelium of $Lysm^+FBXW7^{f/f}$ mice (Fig. 1b). The kidney mediates the balance of waste excretion, electrolytes, and water, and regulates RBC production and systemic blood pressure; these physiological functions rely on the integrity of the renal structure.[38] We found that compared with $Lysm^+FBXW7^{f/f}$ mice, TMPD-injected $FBXW7^{f/f}$ mice exhibited more cell infiltration in the glomeruli and severe glomerulonephritis (Fig. 1c). Then, we analyzed the kidney histology under an electron microscope, and the results revealed an increase in the glomerular mesangial membrane thickness in $FBXW7^{f/f}$ mice (Fig. 1d) and more serious damage to the glomerular podocytes in $FBXW7^{f/f}$ mice (Fig. 1d). Meanwhile, the kidney damage was significantly ameliorated in $Lysm^+FBXW7^{f/f}$ mice (Fig. 1d). Immune complex deposition in the kidney and inflammatory cell infiltration are vital characteristics of lupus nephritis, and inflammatory cell infiltration plays a key role in the pathogenesis of SLE.[39] Monocytes/macrophages and dendritic cells have been reported to infiltrate into the kidney during lupus glomerulonephritis, and neutrophils supposedly play a dominant role in the progression of renal failure.[39] Kidney cells were isolated from $FBXW7^{f/f}$ and $Lysm^+FBXW7^{f/f}$ mice after the 6-month TMPD challenge, and renal infiltration by immune cells was analyzed by flow cytometry. Consistent with the results shown in Fig. 1c, more infiltrated immune cells were observed in the kidney after the 6-month TMPD challenge (Fig. 1e). Compared with $FBXW7^{f/f}$ mice, an evident decrease in the infiltration of dendritic cells ($CD11C^+$), macrophages ($F4/80^+$), and neutrophils ($Ly6G^+$) was observed in $Lysm^+FBXW7^{f/f}$ mice (Fig. 1e), and the monocytes ($Ly6C^+$) were also decreased, although the difference was not significant (Fig. 1e). Taken together, these results suggest that *FBXW7* deficiency in myeloid cells plays a protective role in the pathogenetic process of mice lupus nephritis.

Lack of *FBXW7* alleviated autoimmune responses in mice following TMPD exposure

Over the past 50 years, the long-term survival rate of patients with SLE has improved, and the 5-year survival rate has increased from 74.8% in the 1950s to 94.8% in the 2000s, while the 10-year survival rate has increased from 63.2% to 91.4%.[40] Active SLE, infections, renal failure, and cardiovascular events are the causes of death among patients with SLE.[41] The survival rate of $FBXW7^{f/f}$ and $Lysm^+FBXW7^{f/f}$ mice treated with TMPD was measured for 6 months. Consistent with the renal damage, the TMPD-injected $Lysm^+FBXW7^{f/f}$ mice showed a remarkably increased survival rate compared with $FBXW7^{f/f}$ mice (Fig. 2a). Similar to other SLE-prone mouse strains, TMPD-induced mice with SLE also develop autoimmune responses and autoantibody production.[19] We collected serum from $FBXW7^{f/f}$ and $Lysm^+FBXW7^{f/f}$ mice after the 6-month treatment with TMPD and measured autoantibody production. The results suggested that the levels of anti-ANA and anti-Sm/RNP antibodies were significantly decreased in $Lysm^+FBXW7^{f/f}$ mice compared with those in $FBXW7^{f/f}$ mice (Fig. 2b); however, we did not find obvious anti-dsDNA antibody production in both $FBXW7^{f/f}$ and $Lysm^+FBXW7^{f/f}$ mice (Fig. 2b). This finding is consistent with previous reports that TMPD could not induce anti-dsDNA IgG antibodies in B6 mice.[15,42] To assess

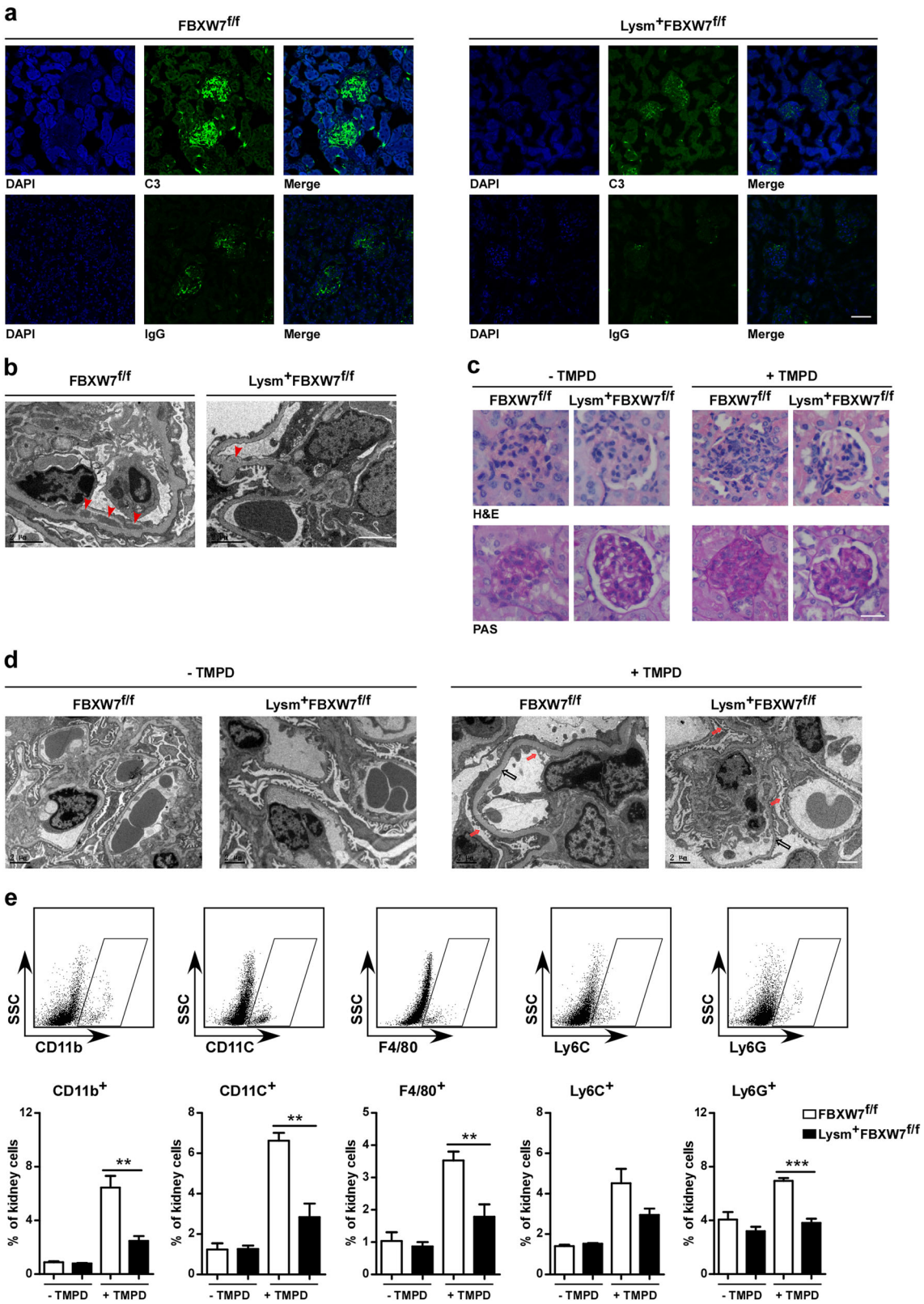

the effects of *FBXW7* deficiency on renal function, the ratio of albuminuria/creatinine in urine was measured 6 months after the TMPD treatment. As expected, this parameter was markedly decreased in Lysm^{+}*FBXW7*$^{f/f}$ mice (Fig. 2c). The spleen is the largest lymphoid organ in the body and is the center of cellular and humoral immunity. After 6 months, splenomegaly was observed in *FBXW7*$^{f/f}$ mice treated with TMPD (Fig. 2d). In parallel, the ratio of spleen/body weight in *FBXW7*$^{f/f}$ mice was also higher

Fig. 1 Lysm^{+}*FBXW7*$^{f/f}$ mice showed decreased renal injury after a 6-month TMPD treatment. **a** Representative images of FITC-conjugated IgG and C3 staining patterns in kidney obtained from TMPD-treated *FBXW7*$^{f/f}$ and Lysm^{+}*FBXW7*$^{f/f}$ mice for 6 months (scale bar, 20 μm). **b** Representative glomeruli in the kidney obtained from TMPD-treated *FBXW7*$^{f/f}$ and Lysm^{+}*FBXW7*$^{f/f}$ mice for 6 months and analyzed under a transmission electron microscope (scale bar, 2 μm). Red arrowheads denote immune complex deposition. **c** Representative glomeruli in the kidney obtained from untreated or TMPD-treated *FBXW7*$^{f/f}$ and Lysm^{+}*FBXW7*$^{f/f}$ mice for 6 months with the indicated dye staining (scale bar, 50 μm). **d** Representative glomeruli in the kidney obtained from untreated or TMPD-treated *FBXW7*$^{f/f}$ and Lysm^{+}*FBXW7*$^{f/f}$ mice for 6 months and analyzed under a transmission electron microscope (scale bar, 2 μm). **e** Flow cytometry and statistical analysis of Ly6G^{+}, Ly6C^{+}, and F4/80^{+} cells in kidneys from untreated or TMPD-treated *FBXW7*$^{f/f}$ and Lysm^{+}*FBXW7*$^{f/f}$ mice for 6 months. The data are expressed as the mean ± s.e.m. and are representative of three independent experiments. $^{**}p < 0.01$; $^{***}p < 0.001$

than that in Lysm^{+}*FBXW7*$^{f/f}$ mice (Fig. 2d). Subsequently, we analyzed lymphocyte activation in the spleen from TMPD-treated mice. Although the percentages of CD19^{+}, CD4^{+}, and CD8^{+} lymphocytes were comparable among all groups (Fig. 2e, f), we found that the expression of major histocompatibility complex II (MHC II) in the CD19^{+} B cells in *FBXW7*$^{f/f}$ mice was strikingly higher than that in Lysm^{+}*FBXW7*$^{f/f}$ mice after the TMPD treatment (Fig. 2g), suggesting that the autoimmune reaction in *FBXW7*$^{f/f}$ mice had an over-activation status. Consistently, the number of plasma cells in the spleens from *FBXW7*$^{f/f}$ mice was also higher than that in Lysm^{+}*FBXW7*$^{f/f}$ mice (Fig. 2h), highlighting the downregulated ability of self-antibody production in Lysm^{+}*FBXW7*$^{f/f}$ mice. Altogether, these data indicate that Lysm^{+}*FBXW7*$^{f/f}$ mice exhibited attenuated autoimmune responses after the TMPD injection.

TMPD-induced peritoneal cell apoptosis was inhibited in Lysm^{+}*FBXW7*$^{f/f}$ mice

Following the i.p. injection of TMPD, abundant inflammatory cells were recruited to the inflamed peritoneal cavity and underwent apoptosis.[19] TMPD-induced peritoneal cell apoptosis in vivo is a crucial event in the self-tolerance breaking and pathogenesis of SLE, which are considered a critical source of autoantigens.[20,21] Two weeks after the TMPD injection, all cells were collected from the peritoneal cavity, and the apoptotic cells were analyzed by flow cytometry. The proportion of apoptotic cells was increased after the TMPD treatment (Fig. 3a, b), and Lysm^{+}*FBXW7*$^{f/f}$ mice showed a significantly decreased ratio of cell apoptosis compared to that of *FBXW7*$^{f/f}$ mice (Fig. 3a, b). Increased apoptotic and dead cells lead to the exposure of nucleic acids and associated nuclear proteins to innate immune cells, resulting in IFN-I and proinflammatory cytokine production through PRRs.[43] Next, we analyzed the peritoneal cells recruited from the periphery and found that the recruited cells were dominantly CD11b^{+} myeloid cells (Fig. 3c, d). Previous studies have indicated that CD11b^{+}Ly6C^{hi} cells were inflammatory monocytes and dominantly IFN-I-producing cells, whereas CD11b^{+}Ly6G^{+} cells are inflammatory granulocytes.[44,45] There was a marked decrease in the ratio of CD11b^{+}Ly6C^{hi} monocytes in Lysm^{+}*FBXW7*$^{f/f}$ mice compared to that in *FBXW7*$^{f/f}$ mice (Fig. 3c, d). We did not find the same difference in the spleen (Supplementary Fig. 2). The ratio of CD11b^{+}Ly6G^{+} neutrophils from the peritoneal cavity and spleen was also comparable between *FBXW7*$^{f/f}$ and Lysm^{+}*FBXW7*$^{f/f}$ mice (Fig. 3c, d and Supplementary Fig. 2). The TMPD-induced SLE model strictly depends on the IFN-I signaling pathway.[19] *FBXW7*$^{f/f}$ mice showed a higher accumulation of CD11b^{+}Ly6C^{hi} monocytes and a higher induction of IFN-I compared to those of Lysm^{+}*FBXW7*$^{f/f}$ mice (Fig. 3d, e). We collected all peritoneal cells and measured the expression of IFN-stimulated genes (ISGs). The results indicated that the expression of ISGs was increased after TMPD treatment in both *FBXW7*$^{f/f}$ and Lysm^{+}*FBXW7*$^{f/f}$ mice, and *FBXW7*$^{f/f}$ mice showed a higher expression of IFN-α, IRF7, ISG15, and MX1 (Fig. 3e). Collectively, these results illustrate that *FBXW7* deficiency decreased TMPD-induced peritoneal cell apoptosis and IFN-I, suggesting that Lysm^{+}*FBXW7*$^{f/f}$ mice may have an alleviated onset of SLE.

FBXW7 promoted TMDP-induced diffuse pulmonary hemorrhage in vivo

Thoracic diseases, including pleuritis and pulmonary hypertension, often occur in patients with SLE. Only a few patients with SLE develop diffuse pulmonary hemorrhage (DPH), but DPH leads to more than 50% mortality.[46] However, as a critical complication of SLE, the underlying mechanism of DPH has not been illuminated. Previous work reported that TMPD-induced SLE model mice also develop DPH.[46,47] Two weeks after the TMPD injection, the mice were sacrificed, and the lung pathology was examined; the results showed that compared with Lysm^{+}*FBXW7*$^{f/f}$ mice, more *FBXW7*$^{f/f}$ mice developed complete DPH or partial DPH (Fig. 4a, c). Next, we established an index of DPH activity (DPH score) according to erythrocyte infiltration in the lung tissue and found that the DPH score in Lysm^{+}*FBXW7*$^{f/f}$ mice was significantly lower than that in *FBXW7*$^{f/f}$ mice (Fig. 4b, c). Leukocyte recruitment appeared in the lung tissue in both *FBXW7*$^{f/f}$ and Lysm^{+}*FBXW7*$^{f/f}$ mice after the TMPD treatment (Fig. 4b), which has also been found in SLE patients with DPH.[48] To identify the subsets of leukocytes that dominantly mediate mouse DPH, we analyzed the recruited cells in BALF and found increased CD11b^{+}Ly6C^{hi} monocytes in BALF from both *FBXW7*$^{f/f}$ and Lysm^{+}*FBXW7*$^{f/f}$ mice after the TMPD treatment, while a dramatic increase in CD11b^{+}Ly6G^{+} neutrophils was observed in *FBXW7*$^{f/f}$ mice, and the ratio of CD11b^{+}Ly6G^{+} neutrophils in *FBXW7*$^{f/f}$ mice was much greater than that in Lysm^{+}*FBXW7*$^{f/f}$ mice (Fig. 4d, e). The levels of inflammatory cytokines were also measured by ELISA in BALF. Consistent with immune cell infiltration, the IL-6, TNF-α, and CCL2 levels in *FBXW7*$^{f/f}$ mice were significantly higher than those in Lysm^{+}*FBXW7*$^{f/f}$ mice (Fig. 4f). Taken together, these data suggested that *FBXW7* deficiency could protect mice from developing DPH induced by TMPD, and neutrophils might be the dominant cells mediating DPH genesis and development.

FBXW7 promoted TMPD-induced cell apoptosis in vitro

In the TMPD-induced mouse SLE model, cell apoptosis is a key event for the initiation of mouse SLE and a potential source of autoantigens.[20,21] We found more apoptotic cells in *FBXW7*$^{f/f}$ mice than in Lysm^{+}*FBXW7*$^{f/f}$ mice (Fig. 3a, b). We also observed more CD11b^{+}Ly6C^{hi} monocytes in *FBXW7*$^{f/f}$ mice, which could be due to intrinsic or extrinsic reasons. To investigate the mechanisms, we performed chemotaxis assays on BMDMs and CD11b^{+}Ly6C^{hi} monocytes from *FBXW7*$^{f/f}$ and Lysm^{+}*FBXW7*$^{f/f}$ mice. The results showed that *FBXW7* deficiency did not affect the cell chemotaxis ability (Supplementary Fig. 3a). To unambiguously confirm this result, we generated bone marrow chimeric mice (Supplementary Fig. 3b). After a 6-week reconstitution, the mice were treated with TMPD for 2 weeks, and the percentages of CD45.1 and CD45.2 monocytes/neutrophils in the peritoneal cavity and spleen were determined by flow cytometry. We observed that the ratio of CD45.1 and CD45.2 monocytes/neutrophils in the peritoneal cavity and spleen was comparable before and after the TMPD injection (Supplementary Fig. 3c, d), indicating that *FBXW7* deficiency has no effect on the cell chemotaxis ability. CD11b^{+}Ly6C^{hi} monocytes have been shown to be the dominant IFN-I-producing cells in the peritoneal cavity and depend on

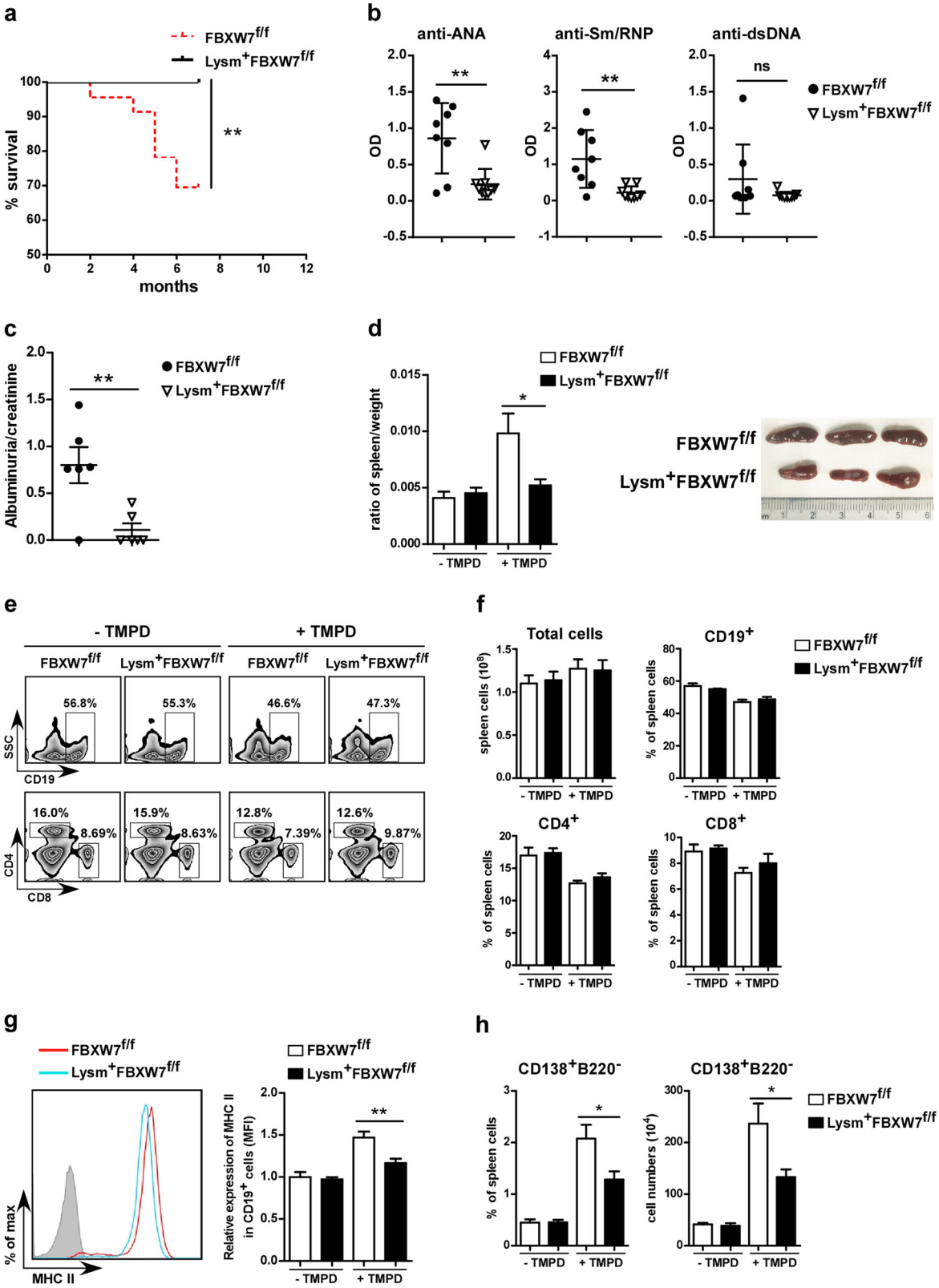

TLR7 signaling.[19,44] Hence, there is another possibility that *FBXW7* may enhance cell immune responses in TLR7-triggered innate immunity. We treated primary macrophages from *FBXW7*$^{f/f}$ and Lysm^{+}*FBXW7*$^{f/f}$ mice with a TLR7 agonist (gardiquimod) and ligand (R848), and measured the production of inflammatory cytokines by ELISA. The results showed that the INF-α, IL-6, TNF-α, and CCL2 levels were similar in the primary macrophages from *FBXW7*$^{f/f}$ or Lysm^{+}*FBXW7*$^{f/f}$ mice (Supplementary Fig. 4a). To confirm this phenomenon in vivo, we challenged *FBXW7*$^{f/f}$ and Lysm^{+}*FBXW7*$^{f/f}$ mice with a lethal dose of the TLR7 agonist

Fig. 2 Lysm^{+}*FBXW7*$^{f/f}$ mice exhibited less autoantibody production and lower lymphocyte activation. **a** Survival curve of TMPD-treated *FBXW7*$^{f/f}$ ($n = 23$) and Lysm^{+}*FBXW7*$^{f/f}$ ($n = 23$) mice over 6 months. **b** Serum anti-ANA, Sm/RNP, and dsDNA antibody levels of TMPD-treated (6 months) *FBXW7*$^{f/f}$ and Lysm^{+}*FBXW7*$^{f/f}$ mice. **c** Ratio of urine albuminuria/creatinine obtained from *FBXW7*$^{f/f}$ and Lysm^{+}*FBXW7*$^{f/f}$ mice 6 months after TMPD treatment. **d** Representative images of spleens from TMPD-treated (6 months) *FBXW7*$^{f/f}$ and Lysm^{+}*FBXW7*$^{f/f}$ mice, and analysis of the spleen/weight ratio. **e** Spleen cells from untreated or TMPD-treated (6 months) *FBXW7*$^{f/f}$ and Lysm^{+}*FBXW7*$^{f/f}$ mice were collected and stained with anti-CD19, anti-CD4, and anti-CD8 antibodies. **f** Statistical analysis of **e**. **g** Flow cytometry analyzing the expression of MHC II in CD19^{+} spleen cells. **h** Spleen cells from untreated or TMPD-treated (6 months) *FBXW7*$^{f/f}$ and Lysm^{+}*FBXW7*$^{f/f}$ mice were collected and stained with anti-CD138 and anti-B220 antibodies. Then, the cells were counted and statistically analyzed. The data are expressed as the mean ± s.e.m. and are representative of three independent experiments. *$p < 0.05$; **$p < 0.01$

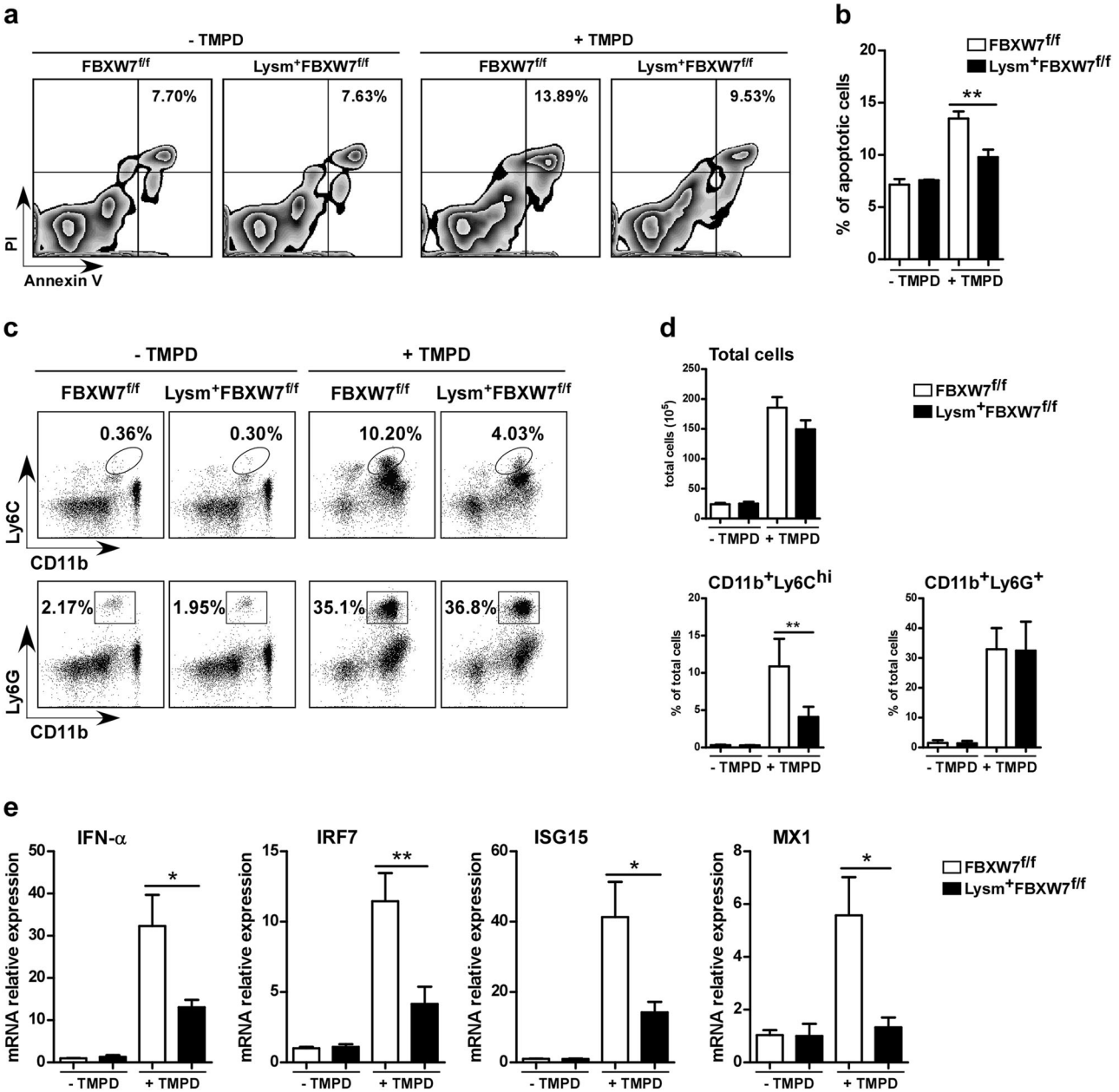

Fig. 3 Lysm^{+}*FBXW7*$^{f/f}$ mice showed reduced cell apoptosis and proinflammatory monocyte infiltration in the peritoneal cavity. **a** All cells were collected from the peritoneal cavity of TMPD-treated (2 weeks) *FBXW7*$^{f/f}$ and Lysm^{+}*FBXW7*$^{f/f}$ mice and stained with anti-Annexin V and PI; then, cell apoptosis was analyzed by flow cytometry. **b** Statistical analysis of **a**. **c** Total number of cells collected from the peritoneal cavity of untreated or TMPD-treated *FBXW7*$^{f/f}$ and Lysm^{+}*FBXW7*$^{f/f}$ mice (for 2 weeks) and stained with anti-CD11b, anti-Ly6C, and anti-Ly6G antibodies; the cells were analyzed by flow cytometry. **d** Statistical analysis of **c**. **e** All cells were collected from the peritoneal cavity of untreated or TMPD-treated *FBXW7*$^{f/f}$ and Lysm^{+}*FBXW7*$^{f/f}$ mice for 2 weeks, and the IFN-α, IRF7, ISG15, and MX1 expression levels were analyzed by qRT-PCR. The data are expressed as the mean ± s.e.m. and are representative of three independent experiments. *$p < 0.05$; **$p < 0.01$

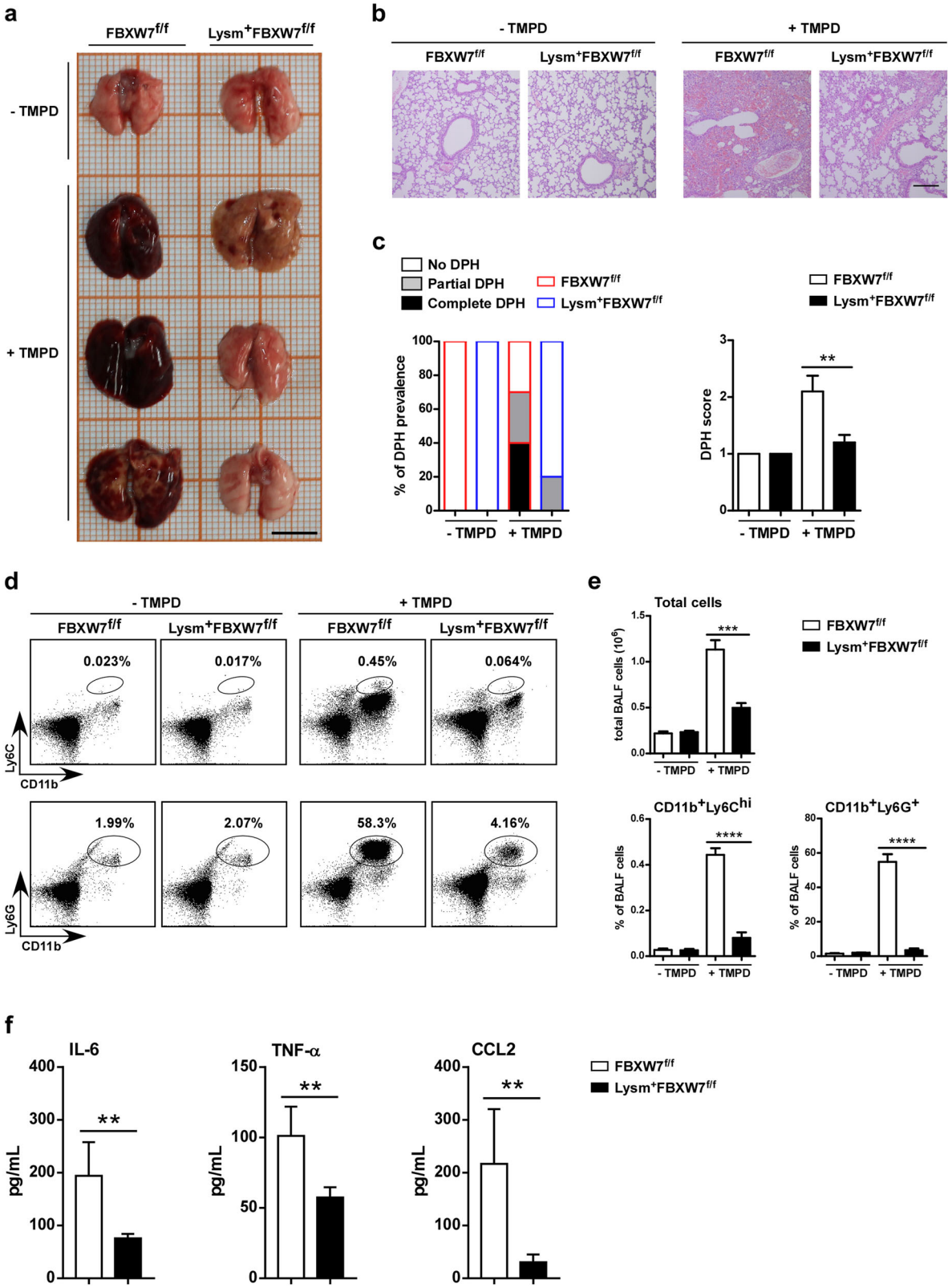

Fig. 4 Lysm^{+}*FBXW7*$^{f/f}$ mice showed reduced CD11b^{+}Ly6G^{+} neutrophil infiltration in BALF and alleviated diffuse pulmonary hemorrhage. **a** Representative images of lungs from untreated or TMPD-treated (for 2 weeks) *FBXW7*$^{f/f}$ and Lysm^{+}*FBXW7*$^{f/f}$ mice (scale bar, 0.5 cm). **b** Representative images of H&E staining of lungs from untreated or TMPD-treated *FBXW7*$^{f/f}$ and Lysm^{+}*FBXW7*$^{f/f}$ mice (scale bar, 200 μm). **c** DPH score of untreated or TMPD-treated (for 2 weeks) *FBXW7*$^{f/f}$ and Lysm^{+}*FBXW7*$^{f/f}$ mice (no DPH = 1, partial DPH = 2, and complete DPH = 3). **d** Total number of cells collected from BALF of untreated or TMPD-treated *FBXW7*$^{f/f}$ and Lysm^{+}*FBXW7*$^{f/f}$ mice; the cells were stained with anti-CD11b, anti-Ly6C, and anti-Ly6G antibodies, and then analyzed by flow cytometry. **e** Statistical analysis of **d**. **f** BALF was collected from TMPD-treated (for 2 weeks) *FBXW7*$^{f/f}$ and Lysm^{+}*FBXW7*$^{f/f}$ mice, and the CCL2, IL-6, and TNF-α levels were measured by ELISA. The data are expressed as the mean ± s.e.m. and are representative of three independent experiments. $^{**}p < 0.01$; $^{***}p < 0.001$; $^{****}p < 0.0001$

and found no significant difference in the survival rate (Supplementary Fig. 4b). The production of IFN-α, IL-6, and TNF-α in the serum of *FBXW7*$^{f/f}$ and Lysm^{+}*FBXW7*$^{f/f}$ mice was also comparable following an injection of a non-lethal dose of the TLR7 agonist (Supplementary Fig. 4c). These results suggest that *FBXW7* deficiency did not affect TLR7-triggered innate immune responses in vitro and in vivo. Thus, the decreased CD11b^{+}Ly6C^{hi} monocyte infiltration and lower expression level of IFN-I in Lysm^{+}*FBXW7*$^{f/f}$ mice are probably due to decreased cell apoptosis, which downregulates autoantigens and triggers immune responses.

Subsequently, we carried out an in vitro assay to confirm the regulation of TMPD-induced cell apoptosis by *FBXW7*. TMPD is an isoalkane with extreme hydrophobicity; thus, we delivered TMDP into cell culture media by using the TMPD inclusion method.[49] TMPD induces cell apoptosis through mitochondrial pathways, including the externalization of membrane phospholipid phosphatidylserine, activation of caspase-3, and cytochrome C release.[21] The primary macrophages were treated with TMPD, and the macrophages from Lysm^{+}*FBXW7*$^{f/f}$ mice showed significantly decreased cell apoptosis (Fig. 5a). The ratio of Bax/Bcl2 and caspase-3 activation level were also higher in *FBXW7*$^{f/f}$ peritoneal macrophages (Fig. 5e, f), and similar results were observed in BMDMs (Fig. 5g). The recruited cells in the peritoneal cavity after the TMPD injection were dominantly CD11b^{+} myeloid cells, including monocytes/macrophages and neutrophils (Fig. 3c, d). The Lysm-Cre mice could also experience an *FBXW7* deletion in neutrophils, and neutrophil apoptosis plays a vital role in SLE progression.[20] Therefore, we isolated bone marrow neutrophils and performed an apoptosis assay; the neutrophil result was similar to that of the macrophages (Fig. 5c, d), indicating that both macrophage and neutrophil apoptosis could contribute to lupus progression. To better implicate *FBXW7* regulation in TMPD-induced apoptosis, we transfected an *FBXW7* plasmid into HeLa cells and treated the cells with TMPD. The results indicate that the overexpression of *FBXW7* results in higher levels of cleaved caspase-3 following TMPD treatment (Fig. 5h). The flow cytometry analysis also showed that the overexpression of *FBXW7* significantly increased cell apoptosis (Fig. 5i, j).

FBXW7 interacted with MCL1 and catalyzed MCL1 for polyubiquitination

FBXW7, which facilitates the ubiquitination of substrates, needs to first recognize a typical sequence motif of the substrate called the conserved CPD motif. CPDs generally contain an *FBXW7* interaction motif, and at positions "0" and "+4", phosphorylated threonine or serine residues exist. This motif could interact with the phosphate-binding pockets of *FBXW7*.[50] To investigate the underlining mechanism, we reviewed the literature on *FBXW7* in the regulation of cell apoptosis and found that myeloid cell leukemia 1 (MCL1) might be the most likely candidate. MCL1 is a pro-survival protein belonging to the BCL2 family, which contains the CPD of *FBXW7* (Fig. 6a). MCL1 could suppress cell apoptosis by inhibiting the activation of pro-apoptotic proteins, including Bax and Bak, and can trigger DNA repair and checkpoint survival signals in the nucleus.[51,52] MCL1 was first identified as a substrate of *FBXW7* in T-cell acute lymphoblastic leukemia and other cancer cell lines.[53,54] To verify our speculation, we constructed an MCL1 plasmid and tested whether *FBXW7* could interact with MCL1. The transient transfection of the Flag-*FBXW7* and HA-MCL1 plasmids together and co-immunoprecipitation followed by immunoblotting indicated that *FBXW7* could interact with MCL1 (Fig. 6b). In a reciprocal co-immunoprecipitation followed by an immunoblot assay of the transfection with Flag-MCL1 and HA-*FBXW7*, we observed similar results (Fig. 6c). Using a more physiological approach, we carried out an endogenous co-immunoprecipitation assay to verify their interaction (Fig. 6d). *FBXW7* targets substrates for ubiquitination to govern various cell processes. An assay of 293T cells transfected with the Flag-MCL1, Myc-*FBXW7*, and HA-Ub plasmids showed that MCL1 could be modified by ubiquitination, and the modification of MCL1 was increased in the presence of *FBXW7* in a dose-dependent manner (Fig. 6e). To determine the type of ubiquitination of MCL1 that was modified by *FBXW7*, different mutations of the HA-Ub plasmids were constructed (Fig. 6f). After the transfection of these mutant plasmids along with Flag-MCL1 and Myc-*FBXW7* in 293T cells, we confirmed that *FBXW7* could promote MCL1 for ubiquitination (Fig. 6g). When lysine at the site of 48 (K48) was mutated in the HA-Ub plasmid, the level of MCL1 ubiquitination catalyzed by *FBXW7* was significantly decreased, but no change was observed when K63 was mutated (Fig. 6g). To confirm the CPD position in MCL1, we constructed a mutant MCL1 plasmid in which serine at position 140 and threonine at position 144 were replaced by glycine. The result showed that *FBXW7* could not catalyze the mutant MCL1 for ubiquitination (Fig. 6h), suggesting that this was a degron sequence. The in vitro ubiquitination assay showed that *FBXW7* could promote MCL1 for ubiquitination (Fig. 6i), indicating that *FBXW7* is an E3 ligase of MCL1. Collectively, these data suggest that *FBXW7* interacts with MCL1 and targets MCL1 for K48-linked ubiquitination.

FBXW7 promoted TMPD-induced cell apoptosis by targeting MCL1 for degradation

MCL1 is frequently overexpressed in various cancer cells; meanwhile, MCL1 exhibits an extremely unstable nature.[53] A previous report showed that *FBXW7* mutations lead to decreased interaction between *FBXW7* and MCL1, and the depletion of endogenous *FBXW7* components increased MCL1 abundance.[53] In the peritoneal macrophages from *FBXW7*$^{f/f}$ and Lysm^{+}*FBXW7*$^{f/f}$ mice, we found that *FBXW7* deficiency could decrease cell apoptosis and increase the abundance of MCL1 (Fig. 7a). In addition, the half-life of MCL1 was markedly reduced in *FBXW7*$^{f/f}$ macrophages compared to that in Lysm^{+}*FBXW7*$^{f/f}$ macrophages (Fig. 7b, c). The overexpression of *FBXW7* in HeLa cells decreased the MCL1 abundance in a dose-dependent manner (Fig. 7d). The overexpression of *FBXW7* in HeLa cells and 293T cells could reduce the half-life of MCL1 (Fig. 7e, f). To better illustrate the role of *FBXW7* in controlling MCL1 stability in myeloid cells, we constructed a lentivirus *FBXW7* and MCL1 plasmids and transfected these constructs into THP-1 cells. As expected, we observed the same results as that observed in the 293T and HeLa cells (Fig. 7g). Protein degradation in eukaryotic cells is mediated by proteases mainly through UPS or autophagy-lysosome system.[55] Our results showed that *FBXW7* catalyzed MCL1 for K48-linked ubiquitination (Fig. 6g); thus, we assumed that MCL1 degradation mediated by *FBXW7* was achieved through UPS. The Flag-MCL1 and Myc-*FBXW7* plasmids were co-transfected into HeLa cells, and the cells were treated with different chemical reagents. We found that the MCL1 protein level was reduced when *FBXW7* was co-expressed but not in the F-box deletion version (Fig. 7h). MCL1 accumulated in the presence of the proteasome system inhibitor MG132 (Fig. 7h); however, the autophagy inhibitors BFA (bafilomycin A.) and chloroquine had no effect on MCL1 stabilization (Fig. 7h). This result confirmed that MCL1 was degraded mainly through UPS catalyzed by *FBXW7*. To prove that MCL1 mediates *FBXW7* function in promoting cell apoptosis, Flag-MCL1 and Myc-*FBXW7* plasmids were transfected into HeLa, and the cells were treated with TMPD to induce cell apoptosis. The result showed that cell apoptosis was significantly decreased when Flag-MCL1 was overexpressed alone (Fig. 7i, j). Meanwhile, when Myc-*FBXW7* was co-expressed in HeLa cells, cell apoptosis recovered (Fig. 7i, j). Taken together, these results suggest that *FBXW7* facilitates cell apoptosis by targeting MCL1 for degradation.

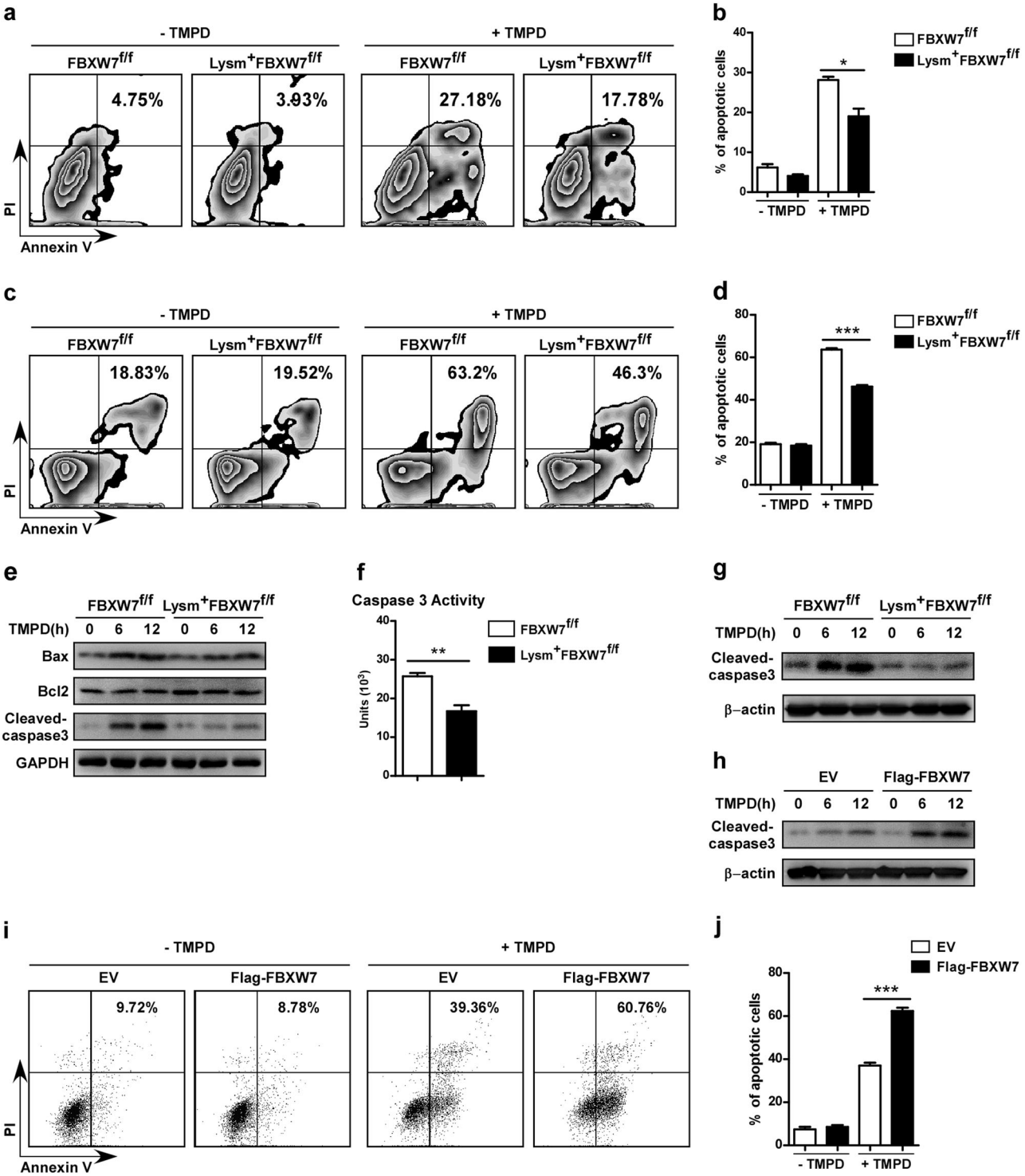

Fig. 5 *FBXW7* promotes TMPD-induced cell apoptosis. **a** *FBXW7* WT and deficient peritoneal macrophages were stained with Annexin V and PI after a treatment with TMPD (200 μM) for 12 h and analyzed by flow cytometry. **b** Statistical analysis of **a**. **c** *FBXW7* WT and deficient neutrophils were stained with Annexin V and PI after a treatment with TMPD (100 μM) for 6 h and analyzed by flow cytometry. **d** Statistical analysis of **c**. **e** *FBXW7* WT and deficient peritoneal macrophages were treated with TMPD (200 μM) for the indicated time and detected by immunoblotting with the indicated antibodies. **f** *FBXW7* WT and deficient peritoneal macrophages were treated with TMPD (200 μM) for 12 h, and capase-3 activity was measured by a Caspase-3 Activity Assay Kit. **g** *FBXW7* WT and deficient bone marrow-derived macrophages (BMDMs) were treated with TMPD (200 μM) for the indicated time and analyzed by immunoblotting. **h** HeLa cells transfected with an empty vector or Flag-*FBXW7* plasmids were treated with TMPD (100 μM) for the indicated time and analyzed by immunoblotting. **i** HeLa cells transfected with an empty vector or Flag-*FBXW7* plasmids were treated with TMPD (100 μM) for 12 h and analyzed by flow cytometry. **j** Statistical analysis of **i**. The data are expressed as the mean ± s.e.m. and are representative of three independent experiments. *$p < 0.05$; **$p < 0.01$; ***$p < 0.001$

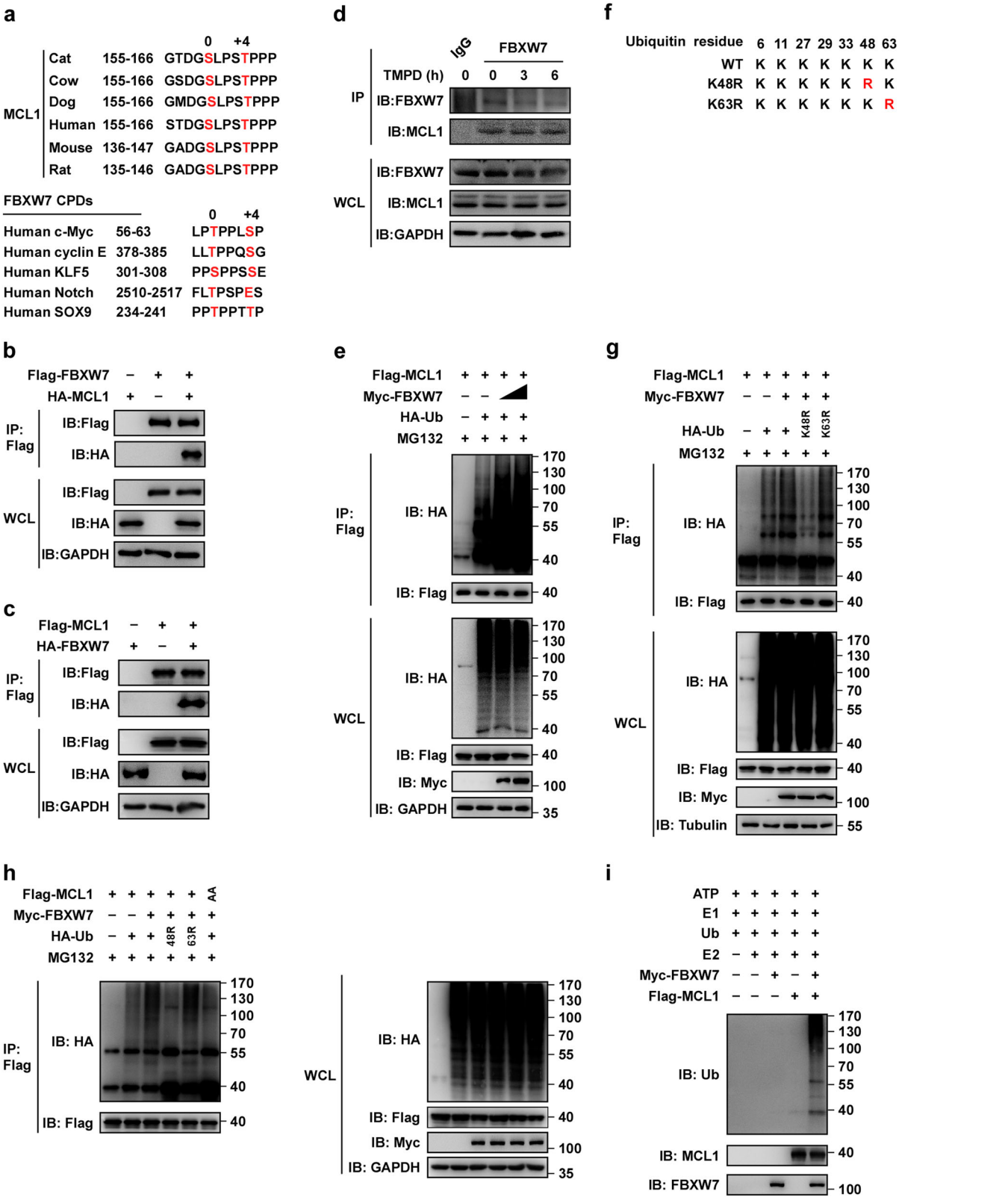

DISCUSSION

In this study, we found that mice with myeloid cell-specific *FBXW7* deficiency (Lysm^{+}*FBXW7*$^{f/f}$) showed attenuated inflammation and immune complex deposition in the kidney. The production of anti-ANA and anti-Sm/RNP antibodies in serum and the albuminuria/creatinine ratio were also decreased in Lysm^{+}*FBXW7*$^{f/f}$ mice. We demonstrated that *FBXW7* plays an important role in promoting TMPD-induced cell apoptosis, which is a crucial event for the pathogenesis of TMPD-induced murine SLE. *FBXW7* could target MCL1 for ubiquitination and subsequent degradation, MCL1 is a key molecule that mediates *FBXW7* function in the regulation of TMDP-induced cell apoptosis.

Fig. 6 *FBXW7* interacts with MCL1 and catalyzes MCL1 for ubiquitination. **a** Sequence alignment of MCL1 with the phosphodegron sequences recognized by *FBXW7* in c-Myc, cyclin E, KLF5, Notch, and SOX9. Putative *FBXW7* phosphodegron sequence present in MCL1 is conserved across different species. Conserved serine and threonine residues within the degron sequences are shown in red. **b** Co-immunoprecipitation and immunoblot analysis of 293T cells co-transfected with Flag-*FBXW7* and HA-MCL1 for 36 h, followed by immunoprecipitation with anti-Flag M2 beads. **c** Co-immunoprecipitation and immunoblot analysis of 293T cells co-transfected with Flag-MCL1 and HA-*FBXW7* for 36 h, followed by immunoprecipitation with anti-Flag M2 beads. **d** Immunoblot analysis of RAW264.7 cells treated with TMPD (100 μM) for the indicated time, followed by immunoprecipitation with *FBXW7*-conjugated agarose or immunoglobulin G (IgG)-conjugated agarose. **e** 293T cells were transfected with Flag-MCL1, Myc-*FBXW7*, and HA-Ub. Cell lysates were subjected to immunoprecipitation with anti-Flag M2 beads and then immunoblotted with the indicated antibodies. **f** Schematic presentation of Ub and its mutants. **g** 293T cells were transfected with Flag-MCL1, Myc-*FBXW7*, and HA-Ub or its mutants. Cell lysates were subjected to immunoprecipitation with anti-Flag M2 beads and then immunoblotted with the indicated antibodies. **h** 293T cells were transfected with Flag-MCL1 or its mutant (AA), Myc-*FBXW7*, and HA-Ub or its mutants. Cell lysates were subjected to immunoprecipitation with anti-Flag M2 beads and then immunoblotted with the indicated antibodies. **i** In vitro ubiquitination assay was performed by incubating purified Flag-MCL1 with ATP, ubiquitin, E1, and E2 in the presence or absence of E2, Myc-*FBXW7*, or Flag-MCL1, followed by immunoblotting

SLE is a heterogeneous chronic autoimmune disease leading to multiple organ damage and even death. The etiological factors of SLE are complex and include autoantigen exposure, hormone level, and environmental factors.[3] Much progress has been achieved by using genetic analyses and mouse models, and these studies have observed that nucleic acid sensing, neutrophil extracellular traps (NETs), IFN production, and lymphocyte signaling were all involved in self-tolerance loss.[3] Notably, increased cell apoptosis and clearance deficiency may initiate innate immunity and have attracted attention due to their contributions to the initiation of human SLE.[5,56]

Although murine lupus models, including spontaneous mouse models and drug-induced models, cannot completely simulate human SLE, there are several common characteristics between these models. In the present study, we built a murine SLE model by TMPD, which replicates various clinical phenotypic and functional abnormalities in human SLE syndrome, including glomerulonephritis, arthritis, autoantibodies, and pericardium inflammation.[19] The i.p. injection of TMPD into normal mice leads to a lupus-like autoimmune syndrome, but the mechanisms that initiate the tolerance loss and lead to autoimmune responses remain to be elucidated. Nicola and colleagues published a study highlighting that cell apoptosis induced by TMPD may provide nuclear autoantigens and their exposure to antigen-presenting cells (APCs), eventually triggering autoimmunity.[21] Another study reported that an intravenous injection of syngeneic apoptotic lymphocytes could induce autoantibody production in mice,[57] suggesting that an excess of cell apoptosis could trigger autoimmune responses. By using a TMPD-induced murine lupus model, a recent study indicated that milk fat globule-epidermal growth factor 8 reduced neutrophil migration, NETosis, and TMDP-induced cell apoptosis, and, thus, suppressed the aberrant immune response in murine SLE, which highlighted neutrophils' contribution to murine lupus.[20] Our study further supports this theory since cell apoptosis, including monocytes/macrophages and neutrophils, in the peritoneal cavity of Lysm^{+}*FBXW7*$^{f/f}$ mice was significantly decreased after the TMPD injection, which eventually reduced self-antibody production and alleviated the kidney injury.

DPH is a rare but life-threatening complication of human SLE that results in capillaritis exclusively in the lung. The clinical symptoms of DPH include capillary wall necrosis, infiltration of inflammatory cells, and hemosiderosis.[58] During the early phase after the TMPD injection, *FBXW7*$^{f/f}$ mice showed significant bleeding into the alveolar space and a large amount of neutrophil aggregation and margination, indicating that *FBXW7* deficiency ameliorated the early DPH phase in the murine SLE model. The pathogenesis of DPH in patients with SLE has not been well characterized since lung biopsy is not routinely performed for diagnosing patients with hemorrhagic complications; thus, uncovering the underlying mechanism is challenging. Although the mechanism of neutrophil infiltration in the lung in this model is not understood, our findings may provide a clue since we observed a dominant subset of neutrophil infiltration, which may mediate DPH.

FBXW7 is among the most frequently mutated genes in human cancers, targeting a network of oncoproteins for degradation, including c-Myc, Notch, and KLF5.[50] By controlling the vital process of the cell cycle, apoptosis, and differentiation, *FBXW7* has become a potential therapeutic target for various human cancers.[29,50] Using an in vitro assay, we confirmed the positive regulatory role of *FBXW7* in TMPD-induced cell apoptosis and found that MCL1 is the target of *FBXW7* during this process. MCL1 has been identified as a substrate of *FBXW7* and plays an anti-apoptosis role in tumor cells;[53,54] however, the precise mechanism is not fully understood. Numerous studies have explored the potential mechanisms of MCL1 in regulating cell apoptosis; for instance, upon irradiation, MCL1 could interact with IEX-1 in the nucleus to stabilize the genome and decrease sensitivity to genotoxic stresses.[51] MCL1 has also been reported to play an anti-apoptotic role in mouse peritoneal macrophages during mycobacterium tuberculosis infection and is considered a crucial factor for neutrophil survival.[59,60] Our study was consistent with these findings because *FBXW7* deficiency caused more MCL1 accumulation and eventually led to reduced cell apoptosis.

Our work has contributed to the understanding of the pathogenesis of SLE to some extent, but more questions still need to be solved. For instance, how TMPD induces the recruitment of monocytes and neutrophils is still unknown. Whether TMPD-induced cell apoptosis is mediated through a cellular receptor and the mechanisms of autoantigen uptake from sustained apoptotic cells leading to a break in self-tolerance and ultimately autoimmunity are also unclear. In summary, we have highlighted the role of *FBXW7* in the pathogenesis of a SLE model and found that *FBXW7* played a crucial role in regulating TMDP-induced cell apoptosis; *FBXW7* absence in myeloid cells resulted in decreased cell apoptosis, autoantibody production, and glomerulonephritis. Hence, *FBXW7* might be used as a potential therapeutic target for SLE prevention and treatment.

ACKNOWLEDGEMENTS

We would like to thank Prof. Ximei Wu for providing the Lysm-Cre mice and Prof. Hong Deng for the kidney pathology analysis. This work was supported by the National Natural Science Foundation of China (81771699, 31870907, and 81571524), Natural Science Foundation of Zhejiang Province (Z19H100001), and National Key Basic Research Program of China (2014CB542101).

ADDITIONAL INFORMATION

The online version of this article (https://doi.org/10.1038/s41423-018-0167-z) contains supplementary material.

Competing interests: The authors declare no competing interests.

Publisher's note: Springer Nature remains neutral with regard to jurisdictional claims in published maps and institutional affiliations.

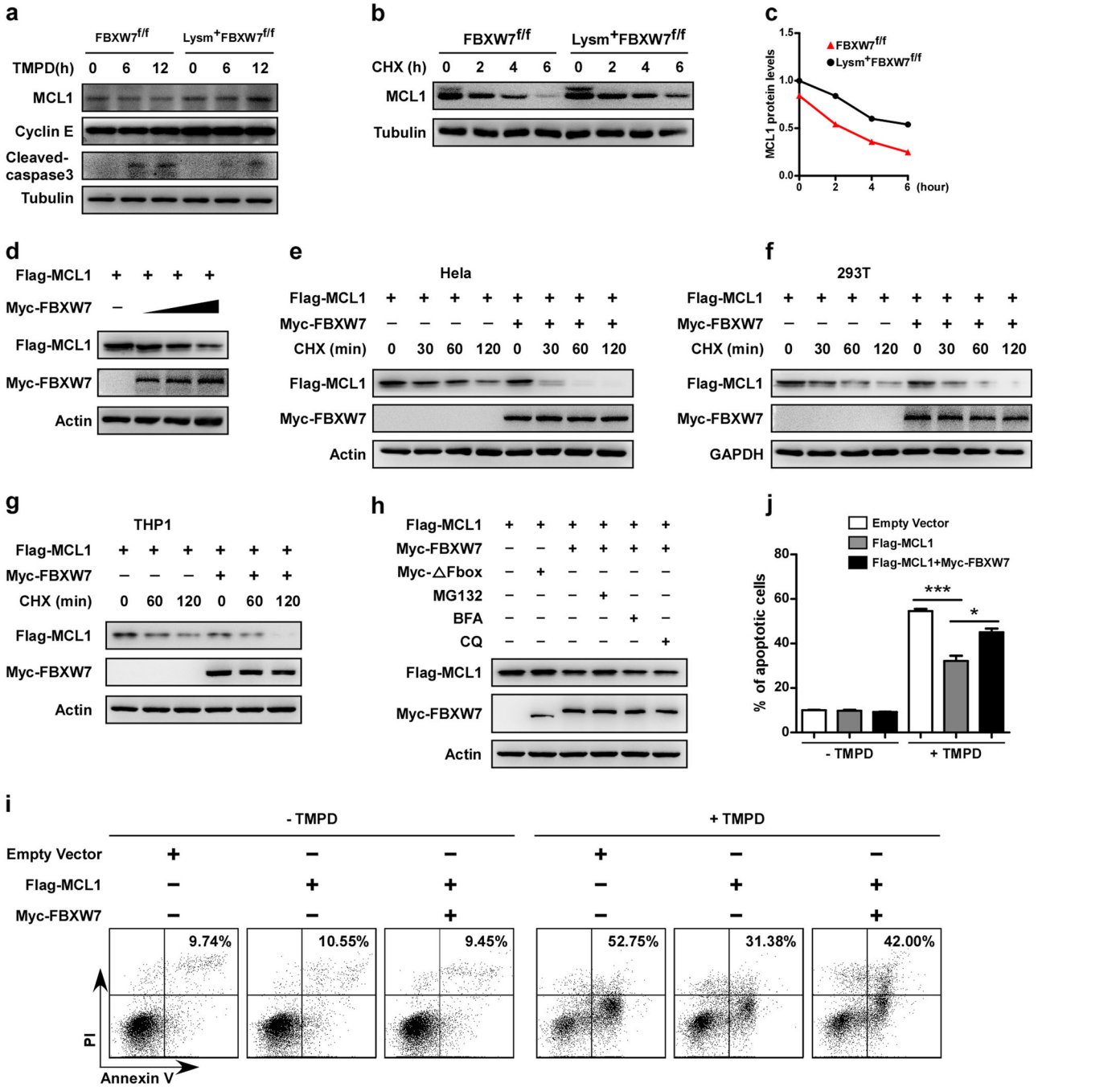

Fig. 7 *FBXW7* targets MCL1 for degradation. **a** *FBXW7* WT and deficient peritoneal macrophages were treated with TMPD (200 μM) for the indicated time and detected by immunoblotting with the indicated antibodies. **b** Immunoblot analysis of MCL1 in lysates of *FBXW7* WT and deficient peritoneal macrophages treated with CHX (20 μg/mL) for the indicated time. **c** Quantification of relative MCL1 levels in **b**. **d** Immunoblot analysis of Flag-MCL1 in lysates of 293T cells co-transfected with Flag-MCL1 and Myc-*FBXW7*. **e** Immunoblot analysis of Flag-MCL1 in lysates of HeLa cells overexpressed with Flag-MCL1 and Myc-*FBXW7*, and treated with CHX (20 μg/mL) for the indicated time. **f** Immunoblot analysis of Flag-MCL1 in lysates of 293T cells overexpressed with Flag-MCL1 and Myc-*FBXW7*, and treated with CHX (20 μg/mL) for the indicated time. **g** Immunoblot analysis of Flag-MCL1 in lysates of THP-1 cells overexpressed with Flag-MCL1 and Myc-*FBXW7*, and treated with CHX (20 μg/mL) for the indicated time. **h** 293T cells transfected with Flag-MCL1, Myc-△F-box, or Myc-*FBXW7* for 24 h, and treated with MG132 (10 μM), BFA (bafilomycin A, 0.2 μM), or CQ (50 μM) for 8 h. The cell lysates were analyzed by immunoblotting. **i** HeLa cells were transfected with an empty vector, Flag-MCL1, and Myc-*FBXW7* plasmids for 36 h, treated with TMPD (100 μM) for 12 h, and analyzed by flow cytometry. **j** Statistical analysis of **i**. The data are expressed as the mean ± s.e.m. and are representative of three independent experiments. *$p < 0.05$; ***$p < 0.001$

REFERENCES

1. Rahman, A. & Isenberg, D. A. Systemic lupus erythematosus. *N. Engl. J. Med.* **358**, 929–939 (2008).
2. Lech, M. & Anders, H. J. The pathogenesis of lupus nephritis. *J. Am. Soc. Nephrol.* **24**, 1357–1366 (2013).
3. Tsokos, G. C., Lo, M. S., Costa Reis, P. & Sullivan, K. E. New insights into the immunopathogenesis of systemic lupus erythematosus. *Nat. Rev. Rheumatol.* **12**, 716–730 (2016).
4. Moulton, V. R. et al. Pathogenesis of human systemic lupus erythematosus: a cellular perspective. *Trends Mol. Med.* **23**, 615–635 (2017).
5. Mahajan, A., Herrmann, M. & Munoz, L. E. Clearance deficiency and cell death pathways: a model for the pathogenesis of SLE. *Front. Immunol.* **7**, 35 (2016).
6. Fenton, K. The effect of cell death in the initiation of lupus nephritis. *Clin. Exp. Immunol.* **179**, 11–16 (2015).
7. Mistry, P. & Kaplan, M. J. Cell death in the pathogenesis of systemic lupus erythematosus and lupus nephritis. *Clin. Immunol.* **185**, 59–73 (2017).
8. Sharma, S., Fitzgerald, K. A., Cancro, M. P. & Marshak-Rothstein, A. Nucleic acid-sensing receptors: rheostats of autoimmunity and autoinflammation. *J. Immunol.* **195**, 3507–3512 (2015).
9. Kirou, K. A. et al. Activation of the interferon-alpha pathway identifies a subgroup of systemic lupus erythematosus patients with distinct serologic features and active disease. *Arthritis Rheum.* **52**, 1491–1503 (2005).
10. Baechler, E. C. et al. Interferon-inducible gene expression signature in peripheral blood cells of patients with severe lupus. *Proc. Natl Acad. Sci. USA* **100**, 2610–2615 (2003).
11. Bennett, L. et al. Interferon and granulopoiesis signatures in systemic lupus erythematosus blood. *J. Exp. Med.* **197**, 711–723 (2003).
12. Jonsson, C. A., Erlandsson, M., Svensson, L., Molne, J. & Carlsten, H. Mycophenolate mofetil ameliorates perivascular T lymphocyte inflammation and reduces the double-negative T cell population in SLE-prone MRLlpr/lpr mice. *Cell Immunol.* **197**, 136–144 (1999).
13. Mannoor, M. K. et al. Honeybee royal jelly inhibits autoimmunity in SLE-prone NZB x NZW F1 mice. *Lupus* **18**, 44–52 (2009).
14. Lewis, R. M. et al. Chronic allogeneic disease. I. Development of glomerulonephritis. *J. Exp. Med.* **128**, 653–679 (1968).
15. Satoh, M. et al. Widespread susceptibility among inbred mouse strains to the induction of lupus autoantibodies by pristane. *Clin. Exp. Immunol.* **121**, 399–405 (2000).
16. Wang, Z. et al. Beneficial effect of Bupleurum polysaccharides on autoimmune disease induced by Campylobacter jejuni in BALB/c mice. *J. Ethnopharmacol.* **124**, 481–487 (2009).
17. Lee, P. Y. et al. A novel type I IFN-producing cell subset in murine lupus. *J. Immunol.* **180**, 5101–5108 (2008).
18. Bossaller, L. et al. TLR9 deficiency leads to accelerated renal disease and myeloid lineage abnormalities in pristane-induced murine lupus. *J. Immunol.* **197**, 1044–1053 (2016).
19. Reeves, W. H., Lee, P. Y., Weinstein, J. S., Satoh, M. & Lu, L. Induction of autoimmunity by pristane and other naturally occurring hydrocarbons. *Trends Immunol.* **30**, 455–464 (2009).
20. Huang, W. et al. Milk fat globule-EGF factor 8 suppresses the aberrant immune response of systemic lupus erythematosus-derived neutrophils and associated tissue damage. *Cell Death Differ.* **24**, 263–275 (2017).
21. Calvani, N. et al. Induction of apoptosis by the hydrocarbon oil pristane: implications for pristane-induced lupus. *J. Immunol.* **175**, 4777–4782 (2005).
22. Jiang, X. & Chen, Z. J. The role of ubiquitylation in immune defence and pathogen evasion. *Nat. Rev. Immunol.* **12**, 35–48 (2012).
23. Wang, Z. et al. Tumor suppressor functions of FBW7 in cancer development and progression. *FEBS Lett.* **586**, 1409–1418 (2012).
24. Bednash, J. S. & Mallampalli, R. K. Regulation of inflammasomes by ubiquitination. *Cell Mol Immunol.* **13**, 722–728 (2016).
25. Li, J., Chai, Q. Y. & Liu, C. H. The ubiquitin system: a critical regulator of innate immunity and pathogen-host interactions. *Cell. Mol. Immunol.* **13**, 560–576 (2016).
26. Pickart, C. M. Mechanisms underlying ubiquitination. *Annu. Rev. Biochem.* **70**, 503–533 (2001).
27. Shimizu, Y., Taraborrelli, L. & Walczak, H. Linear ubiquitination in immunity. *Immunol. Rev.* **266**, 190–207 (2015).
28. Chen, Z. J. & Sun, L. J. Nonproteolytic functions of ubiquitin in cell signaling. *Mol. Cell* **33**, 275–286 (2009).
29. Skaar, J. R., Pagan, J. K. & Pagano, M. SCF ubiquitin ligase-targeted therapies. *Nat. Rev. Drug Discov.* **13**, 889–903 (2014).
30. Xie, C. M., Wei, W. & Sun, Y. Role of SKP1-CUL1-F-box-protein (SCF) E3 ubiquitin ligases in skin cancer. *J. Genet. Genomics* **40**, 97–106 (2013).
31. Welcker, M. et al. The Fbw7 tumor suppressor regulates glycogen synthase kinase 3 phosphorylation-dependent c-Myc protein degradation. *Proc. Natl Acad. Sci. USA* **101**, 9085–9090 (2004).
32. Popov, N., Herold, S., Llamazares, M., Schulein, C. & Eilers, M. Fbw7 and Usp28 regulate myc protein stability in response to DNA damage. *Cell Cycle* **6**, 2327–2331 (2007).
33. Strohmaier, H. et al. Human F-box protein hCdc4 targets cyclin E for proteolysis and is mutated in a breast cancer cell line. *Nature* **413**, 316–322 (2001).
34. Koepp, D. M. et al. Phosphorylation-dependent ubiquitination of cyclin E by the SCFFbw7 ubiquitin ligase. *Science* **294**, 173–177 (2001).
35. O'Neil, J. et al. FBW7 mutations in leukemic cells mediate NOTCH pathway activation and resistance to gamma-secretase inhibitors. *J. Exp. Med.* **204**, 1813–1824 (2007).
36. Balamurugan, K. et al. *FBXW7*alpha attenuates inflammatory signalling by downregulating C/EBPdelta and its target gene Tlr4. *Nat. Commun.* **4**, 1662 (2013).
37. Song, Y. et al. E3 ligase *FBXW7* is critical for RIG-I stabilization during antiviral responses. *Nat. Commun.* **8**, 14654 (2017).
38. Ferenbach, D. A. & Bonventre, J. V. Kidney tubules: intertubular, vascular, and glomerular cross-talk. *Curr. Opin. Nephrol. Hypertens.* **25**, 194–202 (2016).
39. Nowling, T. K. & Gilkeson, G. S. Mechanisms of tissue injury in lupus nephritis. *Arthritis Res. Ther.* **13**, 250 (2011).
40. Mak, A. et al. Global trend of survival and damage of systemic lupus erythematosus: meta-analysis and meta-regression of observational studies from the 1950s to 2000s. *Semin. Arthritis Rheum.* **41**, 830–839 (2012).
41. Thomas, G. et al. Mortality associated with systemic lupus erythematosus in France assessed by multiple-cause-of-death analysis. *Arthritis Rheumatol.* **66**, 2503–2511 (2014).
42. Xu, Y. et al. Pleiotropic IFN-dependent and -independent effects of IRF5 on the pathogenesis of experimental lupus. *J. Immunol.* **188**, 4113–4121 (2012).
43. Barrat, F. J., Elkon, K. B. & Fitzgerald, K. A. Importance of nucleic acid recognition in inflammation and autoimmunity. *Annu. Rev. Med.* **67**, 323–336 (2016).
44. Lee, P. Y. et al. TLR7-dependent and FcgammaR-independent production of type I interferon in experimental mouse lupus. *J. Exp. Med.* **205**, 2995–3006 (2008).
45. Bossaller, L. et al. Overexpression of membrane-bound fas ligand (CD95L) exacerbates autoimmune disease and renal pathology in pristane-induced lupus. *J. Immunol.* **191**, 2104–2114 (2013).
46. Zamora, M. R., Warner, M. L., Tuder, R. & Schwarz, M. I. Diffuse alveolar hemorrhage and systemic lupus erythematosus. Clinical presentation, histology, survival, and outcome. *Medicine* **76**, 192–202 (1997).
47. Shi, Y. et al. Pristane-induced granulocyte recruitment promotes phenotypic conversion of macrophages and protects against diffuse pulmonary hemorrhage in Mac-1 deficiency. *J. Immunol.* **193**, 5129–5139 (2014).
48. Primack, S. L., Miller, R. R. & Muller, N. L. Diffuse pulmonary hemorrhage: clinical, pathologic, and imaging features. *Am. J. Roentgenol.* **164**, 295–300 (1995).
49. Janz, S. & Shacter, E. A new method for delivering alkanes to mammalian cells: preparation and preliminary characterization of an inclusion complex between beta-cyclodextrin and pristane (2,6,10,14-tetramethylpentadecane). *Toxicology* **69**, 301–315 (1991).
50. Davis, R. J., Welcker, M. & Clurman, B. E. Tumor suppression by the Fbw7 ubiquitin ligase: mechanisms and opportunities. *Cancer Cell* **26**, 455–464 (2014).
51. Pawlikowska, P. et al. ATM-dependent expression of IEX-1 controls nuclear accumulation of Mcl-1 and the DNA damage response. *Cell Death Differ.* **17**, 1739–1750 (2010).
52. Inuzuka, H. et al. Mcl-1 ubiquitination and destruction. *Oncotarget* **2**, 239–244 (2011).
53. Inuzuka, H. et al. SCF(FBW7) regulates cellular apoptosis by targeting MCL1 for ubiquitylation and destruction. *Nature* **471**, 104–109 (2011).
54. Wertz, I. E. et al. Sensitivity to antitubulin chemotherapeutics is regulated by MCL1 and FBW7. *Nature* **471**, 110–114 (2011).
55. Kwon, Y. T. & Ciechanover, A. The ubiquitin code in the ubiquitin-proteasome system and autophagy. *Trends Biochem. Sci.* **42**, 873–886 (2017).
56. Denny, M. F. et al. Accelerated macrophage apoptosis induces autoantibody formation and organ damage in systemic lupus erythematosus. *J. Immunol.* **176**, 2095–2104 (2006).
57. Mevorach, D., Zhou, J. L., Song, X. & Elkon, K. B. Systemic exposure to irradiated apoptotic cells induces autoantibody production. *J. Exp. Med.* **188**, 387–392 (1998).
58. Cohen, S. Diffuse pulmonary hemorrhage: evolutionary 'flaw' or consequence of evolutionary progress? *Am. J. Med. Sci.* **323**, 130–139 (2002).
59. Murphy, M. P. & Caraher, E. Mcl-1 is vital for neutrophil survival. *Immunol. Res.* **62**, 225–233 (2015).
60. Wang, F. Y. et al. Suppression of Mcl-1 induces apoptosis in mouse peritoneal macrophages infected with Mycobacterium tuberculosis. *Microbiol. Immunol.* **60**, 215–227 (2016).